JGR Space Physics

RESEARCH ARTICLE
10.1029/2024JA033471

Altitude-Dependent Plasma Parameter Variations of Synthetic EISCAT UHF and VHF Incoherent Scatter Spectra Calculated From TIE-GCM Results

Florian Günzkofer[1], Gunter Stober[2,3], Frank Heymann[1], Anders Tjulin[4], and Claudia Borries[1]

[1]Institute for Solar-Terrestrial Physics, German Aerospace Center (DLR), Neustrelitz, Germany, [2]Institute of Applied Physics, Microwave Physics, University of Bern, Bern, Switzerland, [3]Oeschger Center for Climate Change Research, Microwave Physics, University of Bern, Bern, Switzerland, [4]EISCAT Scientific Association, Kiruna, Sweden

Abstract Incoherent scatter radar measurements rely on the application of a priori parameters from empirical models to initialize the analysis of incoherent scatter spectra. Currently, there is a need to transform ionosphere models to enable reliable space weather predictions through data assimilation of observations. Very often the data assimilation relies on electron densities measured with incoherent scatter radars. Erroneous a priori parameters would lead to the assimilation of inaccurate and physically inconsistent data depending on the ionospheric model. It might therefore be beneficial to assimilate the entire radar spectrum and infer the plasma parameters from the assimilated spectrum by applying the a priori parameters as given by the model. To assess the potential assimilation of incoherent scatter spectra into models, we investigate synthetic EISCAT incoherent scatter spectra calculated from TIE-GCM results. At F1 region altitudes, the atomic-to-molecular ion ratio strongly affects the shape of the incoherent scatter spectrum. Since the vertical profiles of the atomic-to-molecular ion ratio are distinctly different in the EISCAT a priori model and TIE-GCM, the assimilation of single plasma parameters induces additional, unbalanced forces into the model. A similar problem arises in the E region due to different ion-neutral collision frequency profiles. These problems could be solved by assimilation of the entire incoherent scatter spectrum followed by an in-model evaluation of the plasma parameters. We demonstrate the effect of different a priori profiles on the spectral analysis and how the derived plasma parameters are changing when leveraging a more comprehensive approach of using forward modeling with TIE-GCM.

Plain Language Summary Forecasting chaotic systems like weather (and also space weather) requires a combination of modeling and observations called *data assimilation*. Incoherent scatter radar measurements are already partly used for data assimilation. However, multiple parameters affect incoherent scatter radar measurements, and single-parameter assimilation might introduce inconsistencies to the model. We investigate the effect of different parameters on the incoherent scatter spectrum across the different regions of the ionosphere. We illuminate the problems that can arise when assimilating these parameters separately rather than the incoherent scatter spectrum as a combination of all parameters.

Key Points:

- Incoherent scatter radar measurements are strongly affected by a priori ionospheric and thermospheric parameters
- Plasma parameters have a varying effect on the synthetic incoherent scatter spectrum calculated from TIE-GCM results at different altitudes
- Assimilating single plasma parameters inferred from incoherent scatter radar measurements introduces model inconsistencies

Correspondence to:
F. Günzkofer,
florian.guenzkofer@dlr.de

Citation:
Günzkofer, F., Stober, G., Heymann, F., Tjulin, A., & Borries, C. (2025). Altitude-dependent plasma parameter variations of synthetic EISCAT UHF and VHF incoherent scatter spectra calculated from TIE-GCM results. *Journal of Geophysical Research: Space Physics*, *130*, e2024JA033471. https://doi.org/10.1029/2024JA033471

Received 29 OCT 2024
Accepted 13 DEC 2024

Author Contributions:
Conceptualization: Florian Günzkofer, Gunter Stober
Data curation: Frank Heymann, Anders Tjulin
Formal analysis: Florian Günzkofer, Anders Tjulin
Funding acquisition: Claudia Borries
Investigation: Gunter Stober, Anders Tjulin
Methodology: Florian Günzkofer, Gunter Stober
Project administration: Claudia Borries
Resources: Frank Heymann
Software: Florian Günzkofer
Supervision: Gunter Stober, Claudia Borries
Validation: Frank Heymann, Anders Tjulin
Visualization: Florian Günzkofer

1. Introduction

Space weather describes the variability of the near-Earth space environment due to more-or-less regular solar variations and intermittent *solar storms*. The *solar-terrestrial coupling* of the solar wind/magnetic field and the Earth's ionosphere-thermosphere-magnetosphere (ITM) system consists of a large number of coupling processes, posing challenges to the predictability of space weather. The reliability of forecasts and nowcasts can be improved through a combination of modeling and observations known as *data assimilation*. Data assimilation has been applied to forecast the terrestrial weather for several decades (e.g., Navon, 2009; Rabier, 2005). As an interesting side-note, data assimilation also was a crucial part of the guidance system of the *Apollo* spacecrafts (Saponaro & Copps, 1970; Suddath et al., 1967). Consequently, data assimilation is a highly important step toward the development of reliable space weather forecasts (e.g., Mehta & Linares, 2018; Schunk et al., 2014, 2016).

The major problem with data assimilation for space weather forecasting is the sparsity of observations in the Earth's ITM system (Palmroth et al., 2021). However, data assimilation is already commonly applied to model certain ITM processes, for example, the *Assimilative Mapping of Ionospheric Electrodynamics (AMIE)* (Richmond & Kamide, 1988) and the *Assimilative Mapping of Geospace Observations (AMGeO)* (Matsuo, 2020)

Writing – original draft:
Florian Günzkofer, Gunter Stober
Writing – review & editing:
Florian Günzkofer, Gunter Stober, Frank Heymann, Anders Tjulin, Claudia Borries

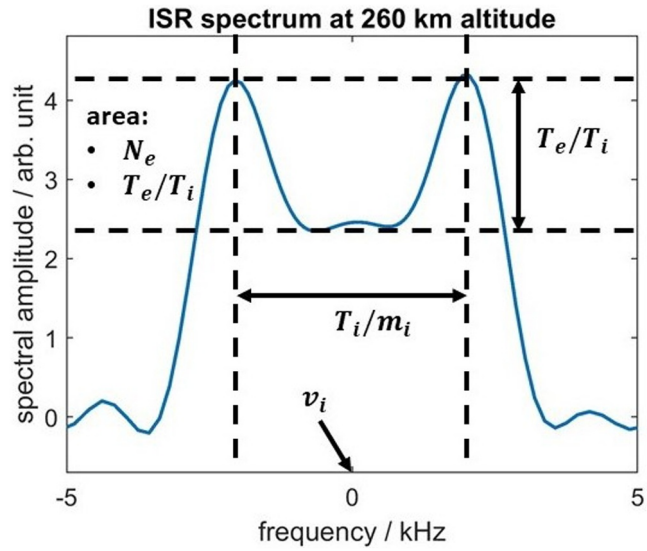

Figure 1. Classical shape of an incoherent scatter spectrum measured with the EISCAT VHF ISR and how various parameters impact the exact shape. From Günzkofer (2024).

which assimilate SuperDARN (Greenwald et al., 1995) and SuperMAG (Gjerloev, 2012) data to describe high-latitude electrodynamics. Since space weather forecasting will require the assimilation of ionosphere and neutral atmosphere parameters with global coverage across all regions of the ionosphere, a large number of data sources is required. Schunk et al. (2014) give an exemplary list of possible data sources.

Incoherent scatter radars (ISRs) provide point measurements; therefore, the global impact of ISR data assimilation in models is presumably limited, although a small integer number of such radars is in operation. A major benefit of ISRs is that they provide vertically resolved profiles of multiple plasma parameters throughout the entire ionosphere with a high time resolution and can therefore play an important role in modeling local effects. There has been a considerable number of studies investigating the assimilation of ISR electron density (e.g., Chartier et al., 2016; Negale et al., 2020; Yue et al., 2007) and ion drift (Hovland et al., 2022; Laundal et al., 2022) measurements. However, there are problems with assimilating only individual plasma parameters derived from ISR measurements. Due to resonant interaction with the ion acoustic wave, the incoherent scatter spectrum contains an *ion line* with a distinct double-peak appearance (Akbari et al., 2017). The exact shape of the ion line depends on many parameters as shown in Figure 1.

The total scatter cross-section and hence the frequency-integrated power of the scatter spectrum is correlated to the electron density N_e. The position of the two peaks is determined by the dispersion relation of the ion acoustic wave. It therefore depends on the ion temperature T_i, the electron temperature T_e, the mean ion mass m_i, and the ion adiabatic coefficient γ_i. γ_i depends on the collisionality of the ionospheric plasma, that is, the ion-neutral collision frequency ν_{in}, and the ion composition due to the different thermodynamic degrees of freedom. Generally, it can be assumed that the three dominant ion species are atomic oxygen O^+ (above about 150 km altitude), as well as molecular oxygen O_2^+ and nitric oxide NO^+ (up to about 250 km altitude) (Baumjohann & Treumann, 1996). The ion composition can be quantified by the ratio of atomic oxygen $r_{O^+} = N_{O^+}/N_e$ and the mean molecular ion mass $A = (30 \cdot N_{NO^+} + 32 \cdot N_{O_2^+})/(N_{NO^+} + N_{O_2^+})$ which can also be applied to express the mean ion mass m_i. The ion acoustic wave is considerably impacted by *Landau damping* which reduces the prominence of the two spectral peaks as well as the frequency-integrated power of the spectrum. The Landau damping is exponentially reduced for $T_e \gg T_i$ (Hutschinson & Freidberg, 2003) but significantly impacts the ion line's shape and the total backscattered power at all altitudes. Lastly, the ISR spectrum can be shifted by a Doppler shift due to the line-of-sight ion velocity v_i. It can be seen that the ion line of the incoherent scatter spectrum is highly complicated which presents the following problems for the assimilation of ISR measurements:

1. Several above-listed parameters have an ambiguous impact on the incoherent scatter spectrum. Therefore, not all parameters are fitted during the ISR analysis process but are taken from empirical a priori models

(Häggström, 2016) (see Section 3). This is mainly the case for the ion-neutral collision frequency ν_{in}, the ratio of atomic oxygen r_{O^+}, and the mean molecular ion mass A. Any inaccuracies of the empirical a priori models result in an inaccurate result of the fitted parameters.

2. The ISR spectrum analysis procedure itself is subject to considerable uncertainties, especially for low spectral amplitudes (low signal-to-noise ratio SNR), that is, at times and altitudes of low electron density. It needs to be considered that the ISR plasma parameters are not directly measured but inferred from measurements of the ISR spectrum.
3. The computational power required for the assimilation of measurements increases with the number of assimilated parameters. Assimilation of each single ISR spectrum parameter is therefore more computationally expensive.

This paper systematically compares measured spectra using EISCAT ultra-high and very-high frequency (UHF and VHF) ISRs with synthetic incoherent scatter spectra calculated from the physics-based thermosphere-ionosphere model TIE-GCM (Richmond et al., 1992). We assess the applicability of ISR spectra as a mapping function to assimilate multiple plasma parameters into a model. Therefore, the sensitivity of the synthetic ISR spectra to plasma parameters at F2, F1, and E region altitudes will be investigated separately. It will be investigated at which altitudes the a priori parameters are of major importance since especially at these altitudes, assimilation of single ISR parameters would be strongly inaccurate causing substantial deviations due to the inconsistencies between the model physics and a priori information.

Section 2 will introduce the EISCAT ISRs and the TIE-GCM. The general uncertainties of the standard EISCAT ISR analysis will be introduced and discussed. Section 3 presents the obtained results for the F2, F1, and E region separately and demonstrates what parameters have a significant impact on the spectrum shape at different altitudes. Section 4 will discuss the obtained results, especially the restrictions of the standard EISCAT ISR analysis and the differences between the two investigated ISRs. Section 5 provides the conclusions and an outlook on potential future work will be given.

2. Measurements and Model

2.1. EISCAT UHF and VHF Incoherent Scatter Radars

Two incoherent scatter radars are operated by the EISCAT Scientific Association near Tromsø, Norway (69.6°N, 19.2°E), the Ultra-High Frequency (UHF, 929 MHz) and the Very-High Frequency (VHF, 224 MHz) radars (Folkestad et al., 1983). The transmission powers of the two ISRs are about $1.5 - 2$ MW for the UHF and about 1.5 MW for the VHF radar respectively. We analyze observations obtained during a 4-hr measurement campaign from 08 to 12 UT on 27 September 2021. This campaign was originally conducted to perform dual-frequency ISR analysis of ion-neutral collision frequencies (Günzkofer et al., 2023). Hence, the UHF and VHF radars are operated in the same operation mode, applying the *beata* pulse code and pointing the radar straight southward at 45° elevation. A summary of all EISCAT instruments, pulse codes, and experimental modes can be found in Tjulin (2022).

EISCAT ISR measurements exhibit altitude-resolved profiles of the electron density N_e, the electron temperature T_e, the ion temperature T_i, and the line-of-sight ion velocity v_i. The Grand Unified Incoherent Scatter Design and Analysis Package (GUISDAP) (Lehtinen & Huuskonen, 1996) is the standard software to fit plasma parameters from ISR spectra. For the analysis presented in this paper, the GUISDAP Version 9.2 was applied. The integration time of the signal auto-correlation function was set to 1 hr. Therefore, plasma parameters are inferred from a 1-hr integration window of radar measurements. Figure 2 shows the ISR spectra measured with the EISCAT UHF and VHF radars from 10 to 11 UT at approximately 120, 200, and 260 km altitude. The fitted spectra obtained from the GUISDAP analysis are shown as well.

It can be seen that the measured UHF spectra in Figure 2a are a bit more noisy compared to the VHF spectra in Figure 2b. However, it can also be seen that the fitted UHF spectra agree considerably better with their measured counterparts than the fitted VHF spectra. In particular, at E region altitudes corresponding to the range gate at 120 km, the measured VHF spectrum shows no clear signature of the characteristic double-peak shape of ISR spectra, while the GUISDAP fit still enforces such a double-peak structure. Deviations of measured and fitted VHF spectra can also be observed at F region altitudes.

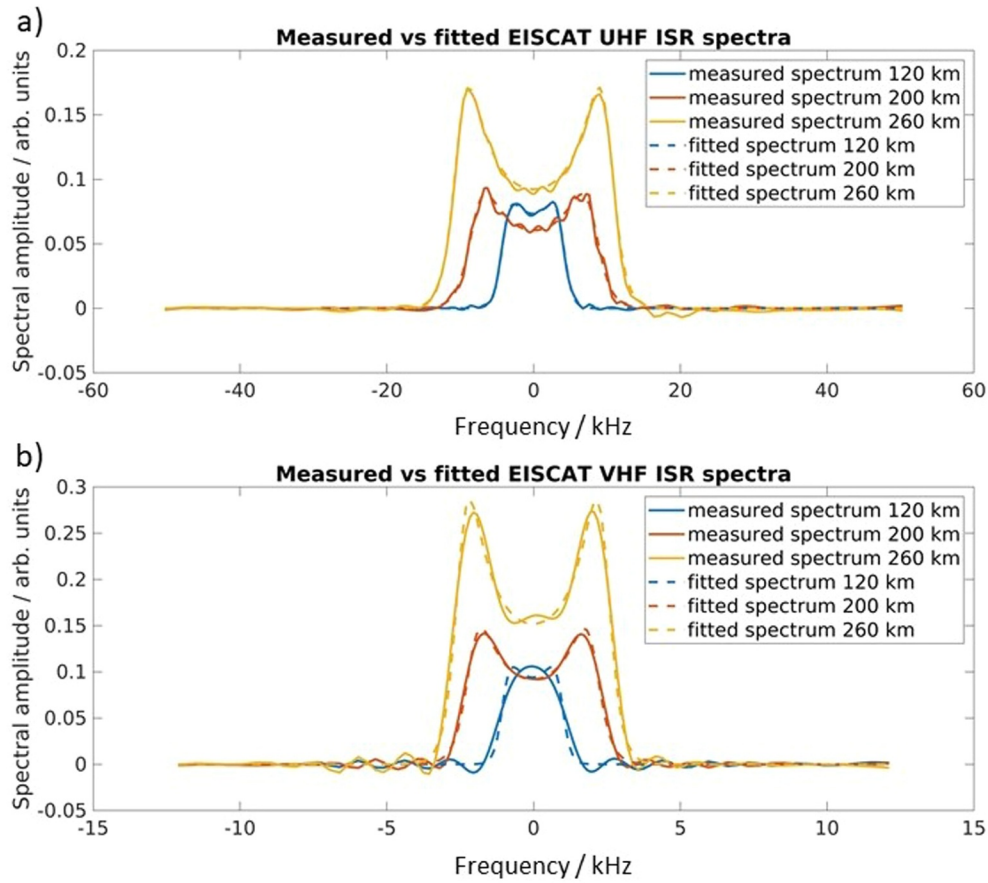

Figure 2. Comparison of measured and GUISDAP fitted EISCAT (a) UHF and (b) VHF spectra averaged from 10 to 11 UT at approximately 120, 200, and 260 km altitude.

For the comparison with synthetic EISCAT spectra calculated from TIE-GCM results, we will apply fitted EISCAT spectra, since the absence of noise will allow for a better assessment of the altitude-dependent impact of various parameters on the spectra. However, for the assimilation of ISR spectra into models, measured spectra would be more suitable than fitted ones. This will be discussed in Section 4.

2.2. TIE-GCM

The Thermosphere Ionosphere Electrodynamics General Circulation Model (TIE-GCM) (Richmond et al., 1992) is a global, physics-based model of the coupled ionosphere-thermosphere system. In this paper, the TIE-GCM version 2.0 is applied. The investigated TIE-GCM output is given on a 2.5°× 2.5° longitude-latitude grid and has a time resolution of 1 hr. The vertical resolution is 1/4 in scale height units ($\sim 2 - 18$ km) and the covered altitudes are $\sim 96 - 530$ km. At the lower boundary, atmospheric dynamics can be driven by the climatologies of several atmosphere models. The TIE-GCM run applied in this paper was generated assuming the tidal dynamics given by the Global Scale Wave Model (Hagan & Forbes, 2002, 2003). The polar plasma convection at high latitudes is driven with the *Heelis* convection model (Heelis et al., 1982).

3. Results

3.1. Measurement and Model Parameters

First, we will look at the parameters that affect the incoherent scatter spectrum, as given by the EISCAT GUISDAP standard analysis and TIE-GCM. Figure 3 shows one-hour-mean vertical profiles of the plasma parameters that are inferred from the shape of the incoherent scatter spectrum.

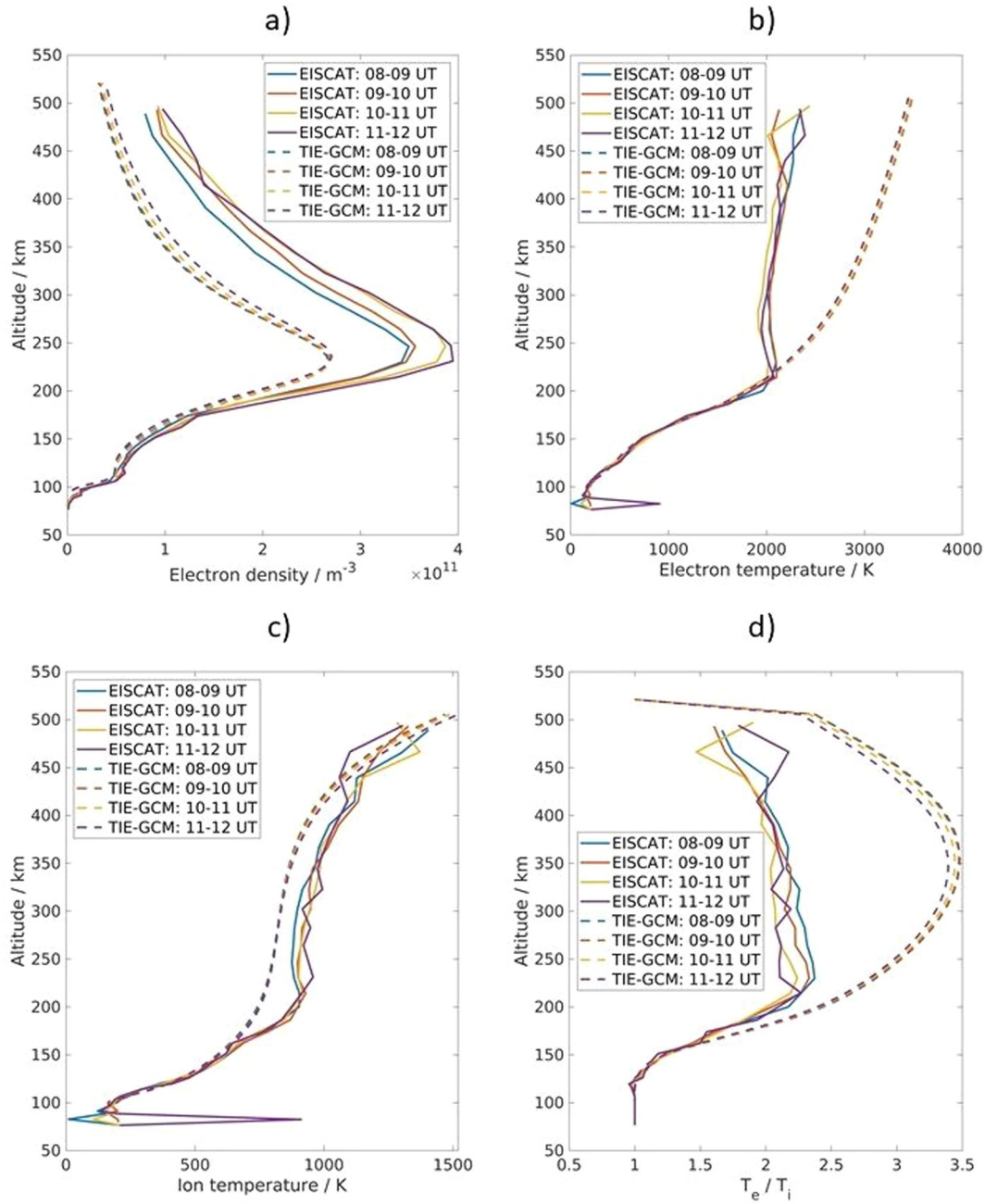

Figure 3. One-hour-mean profiles of the plasma parameters (a) electron density, (b) electron temperature, (c) ion temperature, and (d) ratio of electron-to-ion temperature from EISCAT UHF measurements and TIE-GCM.

In Figure 3a, it can be seen that the EISCAT UHF and TIE-GCM electron densities agree considerably well in the E and F1 regions. However, TIE-GCM underestimates the electron density at the F2 region around the maximum and the topside ionosphere. As expected, both model and measurement show an increase in electron density throughout the investigated 4-hr period from 08 to 12 UT. The electron temperature profiles in Figure 3b show a steady increase of T_e with altitude for TIE-GCM. The EISCAT measurements exhibit a local maximum of T_e in the lower F region and lower electron temperatures for the topside ionosphere compared to the model. The ion temperatures in Figure 3c show a generally good agreement of measurement and model. As described in Section 1, the ratio of electron-to-ion temperatures T_e/T_i is important for the Landau damping of the ion acoustic wave and therefore strongly affects the shape of the incoherent scatter spectrum. Figure 3d shows the vertical

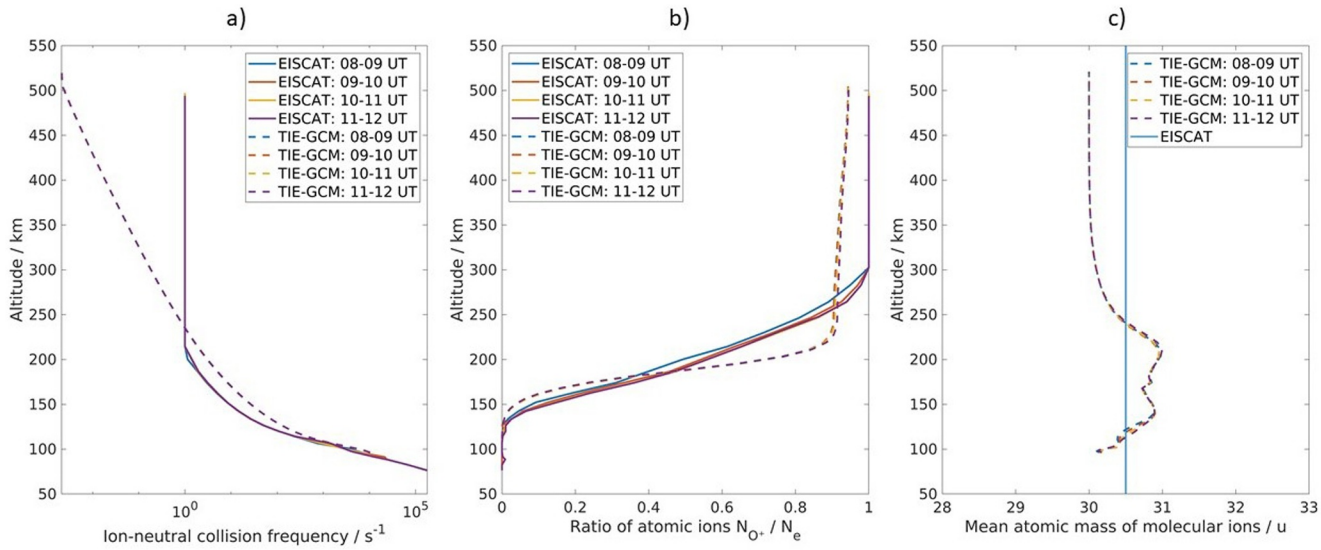

Figure 4. One-hour mean profiles of the (a) ion-neutral collision frequency, (b) ratio of atomic ions, and (c) mean mass of molecular ions from the EISCAT models and from TIE-GCM.

profiles of T_e/T_i, which is considerably larger in the model compared to the EISCAT measurements above the E region.

There are also physical parameters that affect the incoherent scatter spectrum that are pre-described in the ISR analysis process such as the ion-neutral collision frequency, the mean atomic mass, and the ratio of atomic ions to electrons, which are shown in Figure 4. The EISCAT-labeled profiles in Figure 4 are taken from empirical a priori models and applied during the fitting of the incoherent scatter spectra. The ion composition is obtained from the *International Reference Ionosphere (IRI)* (Bilitza et al., 2022; Rawer et al., 1978). The full installation of the GUISDAP version 9.2 software includes a compiled version of the IRI version 2020. It should be noted that depending on the GUISDAP installation, older IRI versions are applied as an empirical ionosphere model, which may result in considerable deviations. The ion-neutral collision frequency is calculated from the empirical neutral atmosphere given by the *NRLMSIS* model (Picone et al., 2002) though older GUISDAP installations might apply the *CIRA* model (Rees & Fuller-Rowell, 1988). The profiles of a priori parameters are stored in the GUISDAP output files as described in Häggström (2016).

The ion-neutral collision frequency ν_{in} in Figure 4a shows notable differences between TIE-GCM and the EISCAT a priori profile in the E and lower F region. The EISCAT ISR analysis software GUISDAP limits the ion-neutral collision frequency to a minimum of 1 s^{-1}. This leads to significant deviations from the TIE-GCM results in the upper F region and topside ionosphere. However, since ν_{in} decreases exponentially with altitude, the ionosphere is presumably completely collision-less at the F region altitudes and above and therefore the limitation to a minimum value has no relevant impact on the incoherent scatter spectrum. The ratio of atomic oxygen $r_{O^+} = N_{O^+}/N_e$ is shown in Figure 4b. The EISCAT a priori profile indicates that the ionosphere plasma is completely molecular up to about 125 km and mostly atomic above about 275 km altitude. The TIE-GCM results show a distinctly different profile, with a completely molecular ionosphere plasma up to about 150 km altitude and a dominantly atomic ionosphere above about 200 km altitude. The transition from a molecular to an atomic plasma is notably sharper in TIE-GCM than assumed by the EISCAT a priori model. This affects both the mean ion mass m_i and the ion adiabatic coefficient γ_i and therefore also the incoherent scatter spectrum. The mean molecular ion mass, which essentially quantifies the ratio of O_2^+ and NO^+, is shown in Figure 4c. The EISCAT ISR analysis assumes a constant mean molecular ion mass of $A = 30.5$ u. As can be seen, TIE-GCM gives a minor variation of 30 u $< A <$ 31 u within proximity to the constant mean molecular ion mass of the EISCAT analysis.

It can be seen from Figure 3 that the main plasma parameters N_e, T_e, and T_i are distinctly different in measurement and model. Since the electron density is generally $N_e > 10^{10}$ m^{-3}, the signal-to-noise ratio of the incoherent

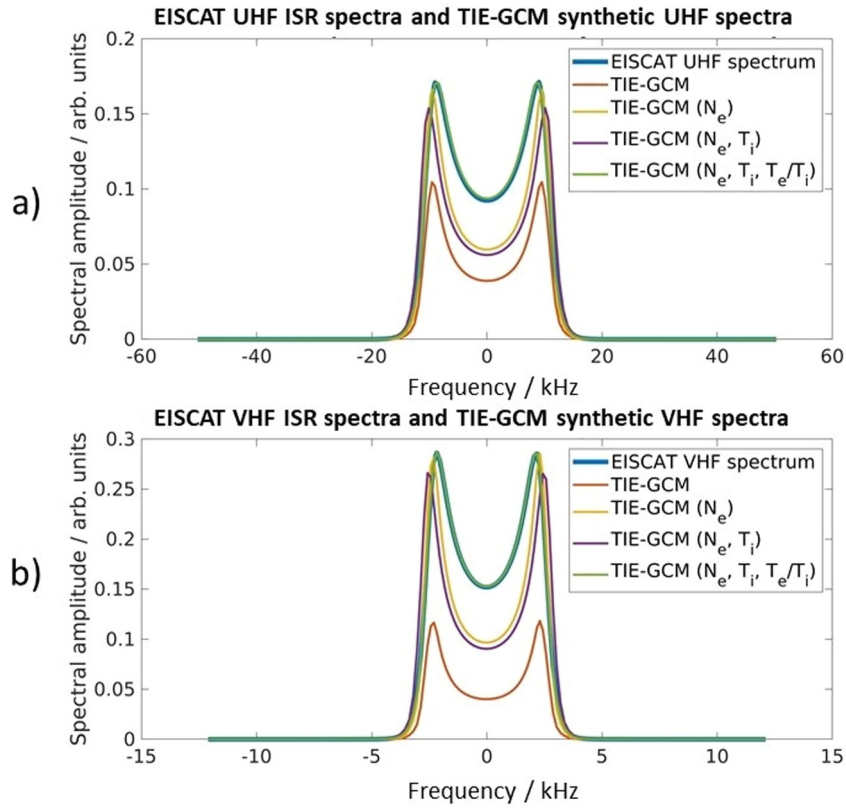

Figure 5. Synthetic (a) UHF and (b) VHF spectra at 260 km altitude at 10–11 UT. The parentheses in the figure legend indicate which parameters have been taken from EISCAT measurements.

scatter measurements is sufficiently high and the ISR plasma parameters are reliable. Hence, an assimilation of ISR measurements into the model would notably improve the model results. On the other hand, Figure 4 shows that the profiles of EISCAT a priori parameters can be quite different from the TIE-GCM profiles. This presumably impacts the parameters in Figure 3 and therefore assimilating one or more of those parameters directly might not result in a more physically realistic state of the model, although some of the parameters are directly assimilated.

In the following sections, we will systematically investigate how synthetic EISCAT spectra are impacted by the parameters in Figures 3 and 4 at F2, F1, and E region altitudes. Since there is little geophysical variation between the four 1-hr intervals from 08 to 12 UT, all comparisons are done for the 10–11 UT interval and are considered representative of the investigated time. We will answer the following questions:

- Can the plasma temperatures be assimilated into a model via the incoherent scatter spectrum or do they not affect the spectrum significantly?
- Do the a priori parameters affect the shape of the spectrum and what parameters are of importance at which altitudes?
- How would the plasma parameters be affected if we were to apply TIE-GCM profiles of the a priori parameters?

3.2. F2 Region

Figure 5 shows the "measured" (i.e., GUISDAP fitted) UHF and VHF incoherent scatter spectra at 260 km altitude for the 1-hr interval from 10 to 11 UT. Synthetic ISR spectra are calculated from TIE-GCM results and shown in Figure 5 as well. A total of four synthetic spectra is calculated, using (a) only TIE-GCM results, (b) the EISCAT electron density, (c) the EISCAT electron density and ion temperature, and (d) the EISCAT electron density, ion, and electron temperature.

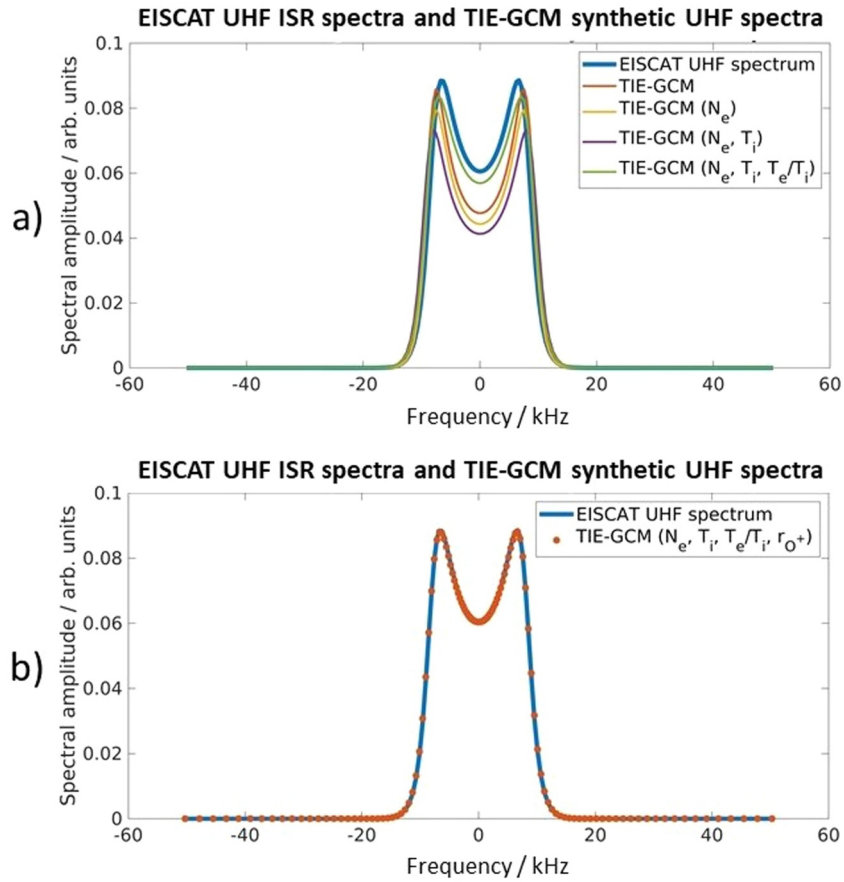

Figure 6. (a) Synthetic UHF spectra at 200 km altitude at 10–11 UT. The parentheses in the figure legend indicate which parameters have been taken from the EISCAT measurements. It can be seen that "measured" and synthetic spectra agree only after the EISCAT a priori ratio of atomic ions has been applied to the calculation.

The impact of the plasma parameters N_e, T_i, and T_e as well as the ratio T_e/T_i on the synthetic ISR spectra are very similar for the UHF and VHF spectra shown in Figures 5a and 5b. The synthetic spectra based on only TIE-GCM parameters have considerably lower signal amplitudes than the corresponding "measured" EISCAT spectra. Applying the EISCAT-measured electron density N_e for the calculation of the synthetic spectra (equivalent to the total assimilation of the model electron density) significantly increases the signal amplitudes of the spectra and the peak signal amplitude is nearly equivalent to the measured spectra. However, the signal power of the minimum between the peaks is considerably lower for the synthetic spectra compared to the measured spectra. Applying the ion temperature T_i for the calculation of the synthetic spectra does not improve the results notably and only after the application of the temperature ratio T_e/T_i our measured and synthetic spectra become equivalent. This indicates that the plasma temperatures T_i and T_e significantly affect the F2 region incoherent scatter spectra. At these altitudes, the ISR spectrum can therefore be applied as a mapping function to assimilate N_e, T_i, and T_e into a model. Also, the differences of a priori parameters applied by GUISDAP and the TIE-GCM do not seem to have a relevant impact on the incoherent scatter spectra at F2 region altitudes. Hence, a separate assimilation of the three plasma parameters would give equivalent results to the assimilation of the incoherent scatter spectra.

3.3. F1 Region

Figures 6 and 7 show the "measured" and synthetic incoherent scatter spectra, analog to Figure 5, at 200 km altitude. Additionally to the three plasma parameters N_e, T_i, and T_e, the impact of the ratio of atomic ions on the synthetic incoherent scatter spectra is also shown in two separate panels for both ISRs.

Figures 6a and 7a show that the synthetic UHF and VHF spectra respond differently to the variation of the plasma parameters N_e, T_i, and T_e. However, the general implications are the same for UHF and VHF spectra. Even for total

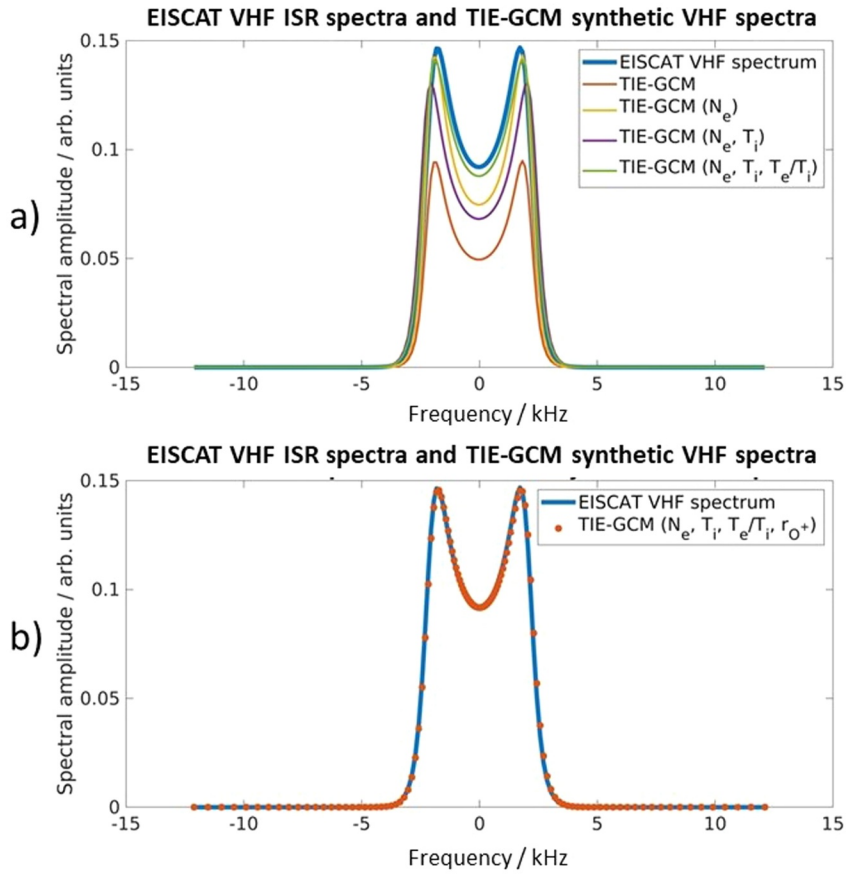

Figure 7. Same as Figure 6 but for VHF.

assimilation of N_e, T_i, and T_e, the synthetic incoherent scatter spectra exhibit substantial discrepancies from the measured spectra. Only after applying also the ratio of atomic ions (i.e., atomic oxygen) r_{O^+}, the synthetic and measured spectra converge and reflect a good agreement as shown in Figures 6b and 7b. Considering all three a priori parameters in Figure 4, only r_{O^+} affects the incoherent scatter spectrum significantly at F1 region altitudes. This is quantitatively shown in Table 1 where the mean squared deviations (MSD) of all synthetic spectra in Figures 6 and 7 are shown. It can be seen that the assimilation of N_e, T_e/T_i, and r_O^+ each reduce the MSD by about one order of magnitude. The assimilation of ν_{in} on the other hand does not have any effect on the spectra in the F1 region.

Table 1
Mean Squared Deviation (MSD) of the "Measured" and Synthetic Spectra Shown in Figures 6 and 7

	MSD F1 UHF	MSD F1 VHF
TIE-GCM	$8 \cdot 10^{-5}$	$1 \cdot 10^{-3}$
TIE-GCM (N_e)	$1 \cdot 10^{-4}$	$1 \cdot 10^{-4}$
TIE-GCM (N_e, T_i)	$2 \cdot 10^{-4}$	$4 \cdot 10^{-4}$
TIE-GCM ($N_e, T_i, T_e/T_i$)	$2 \cdot 10^{-5}$	$4 \cdot 10^{-5}$
TIE-GCM ($N_e, T_i, T_e/T_i, r_O^+$)	$1 \cdot 10^{-7}$	$3 \cdot 10^{-6}$
TIE-GCM ($N_e, T_i, T_e/T_i, \nu_{in}$)	$2 \cdot 10^{-5}$	$4 \cdot 10^{-5}$

Note. The rows show which parameters have been assimilated and all numbers have arbitrary units.

Under the assumption that the TIE-GCM r_{O^+} profile is more accurate than the empirical EISCAT a priori profile, an assimilation of N_e, T_i, and T_e would be inaccurate and induce large imbalances into the model. In Section 4, we will discuss the actual impact on the plasma parameters and thereby quantify the error that would be introduced into the model by the assimilation of single parameters. An assimilation of the incoherent scatter spectrum into the model with an add-on analysis of the synthetic ISR spectrum applying the model profiles for a priori parameters would significantly improve the model results. Moreover, it would improve the overall physical consistency between model and observation.

3.4. E Region

Figures 8 and 9 show the "measured" and synthetic incoherent scatter spectra, analog to Figures 5–7, at 120 km altitude. Additionally to the three plasma parameters N_e, T_i, and T_e, the impact of the ion-neutral collision

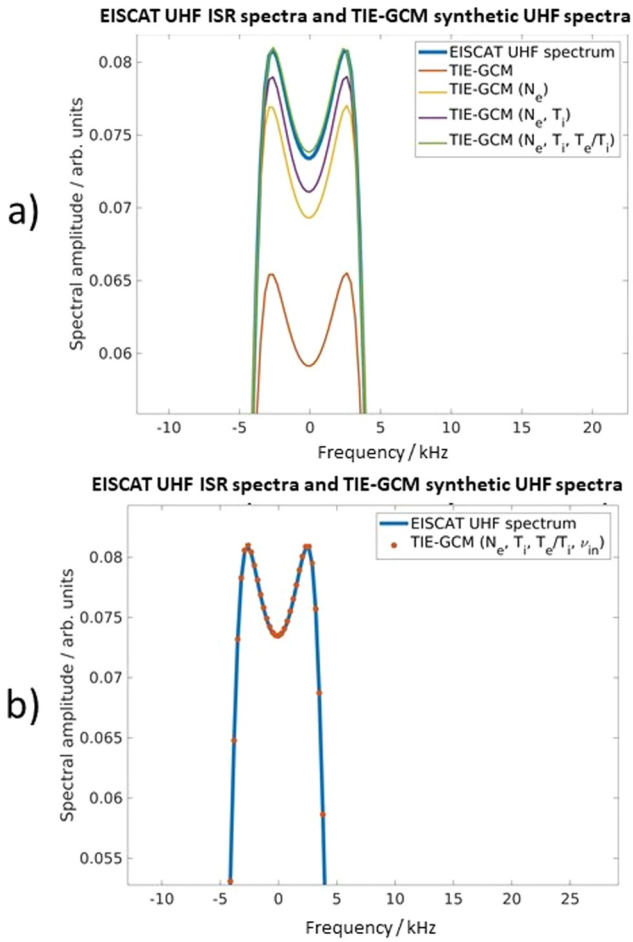

Figure 8. (a) Synthetic UHF spectra at 120 km altitude at 10–11 UT. The parentheses in the figure legend indicate which parameters have been taken from the EISCAT measurements. (b) It can be seen that "measured" and synthetic spectra agree only after the EISCAT a priori ion-neutral collision frequency has been applied to the calculation.

frequency ν_{in} on the synthetic incoherent scatter spectra is shown in two separate panels.

Figures 8a and 9a show that the synthetic incoherent scatter spectra fit the measured spectra considerably better when applying EISCAT plasma parameters during the calculation. For the synthetic UHF spectrum, a total assimilation of N_e and T_i already leads to a synthetic spectrum that resembles the measured one. The similarity is improved further when adding T_e/T_i to the calculation of the synthetic spectrum, though minor deviations remain. For the synthetic VHF spectrum, just assimilating N_e already results in a high similarity of synthetic and measured spectra. However, even after adding both T_i and T_e/T_e to the calculation of the synthetic spectrum, minor deviations remain as well. As shown in Figures 8b and 9b, the remaining discrepancies can be mainly attributed to the ion-neutral collision frequency ν_{in}. Hence, of the three a priori parameters in Figure 4, ν_{in} is the most relevant one at E region altitudes. Generally, the ion-neutral collision frequency can be assumed to have a relevant impact on ionospheric dynamics, and therefore also on the incoherent scatter spectrum, at altitudes up to about 120–130 km. At these altitudes, the ionosphere is considered collisional as the collision frequency is larger than the ion gyro-frequency. However, the impact of ν_{in} on the synthetic incoherent scatter spectra in the E region is notably lower than the impact of r_{O^+} in the F1 region. For low electron density in the E region, the impact of ν_{in} on the incoherent scatter spectrum might be lower than the noise level. Therefore, an assimilation of single parameters N_e, T_i, and T_e should give similar results as a combined assimilation of the incoherent scatter spectra as a mapping function. It has to be remembered though, that the "measured" spectra shown here are the results of the GUISDAP fit of the actually measured spectra which deviate quite notably as shown in Figure 2.

4. Discussion

4.1. Plasma Parameter Profiles for TIE-GCM A Priori Parameters

Figures 6–9 demonstrate that the a priori parameters can affect the incoherent scatter spectrum quite significantly. Especially, the ratio of atomic oxygen in the F1 region appears to have a major impact. While we cannot conclusively determine whether TIE-GCM or the EISCAT a priori model do resemble the actual ion composition more accurately, we can investigate the changes of the ISR plasma parameters assuming that the TIE-GCM profile is correct. By applying a non-linear least square fit, we determined the plasma parameters N_e, T_i, and T_e from the measured incoherent scatter spectra under the assumption of the TIE-GCM profiles for the a priori parameter in Figure 4. Figure 10 shows the resulting profiles of the fitted plasma parameters. It should be noted that a simple non-linear least-square fit is far less sophisticated than the GUISDAP analysis software but appears to be sufficient for an initial comparison.

It can be seen in Figures 10a and 10d that the electron density and T_e/T_i profiles are only changed slightly by the re-evaluation assuming TIE-GCM a priori profiles. However, Figures 10b and 10c show significant changes to the electron and ion temperature profiles. The small local maximum of the electron temperature between 150 and 250 km altitude that has been observed in the default EISCAT profiles (see also Figure 3) disappears in the re-evaluated profiles. It can be seen that the default ion temperature also exhibits a small local maximum in the lower F region which also disappears when applying TIE-GCM as a priori model. At these altitudes, the main impact of the a priori parameters comes from the ratio of atomic oxygen r_{O^+}. Hence, the local maxima of T_e and T_i are directly related to different r_{O^+} profiles in Figure 4b and therefore potential artifacts in case the EISCAT a priori profile causes inaccurate results.

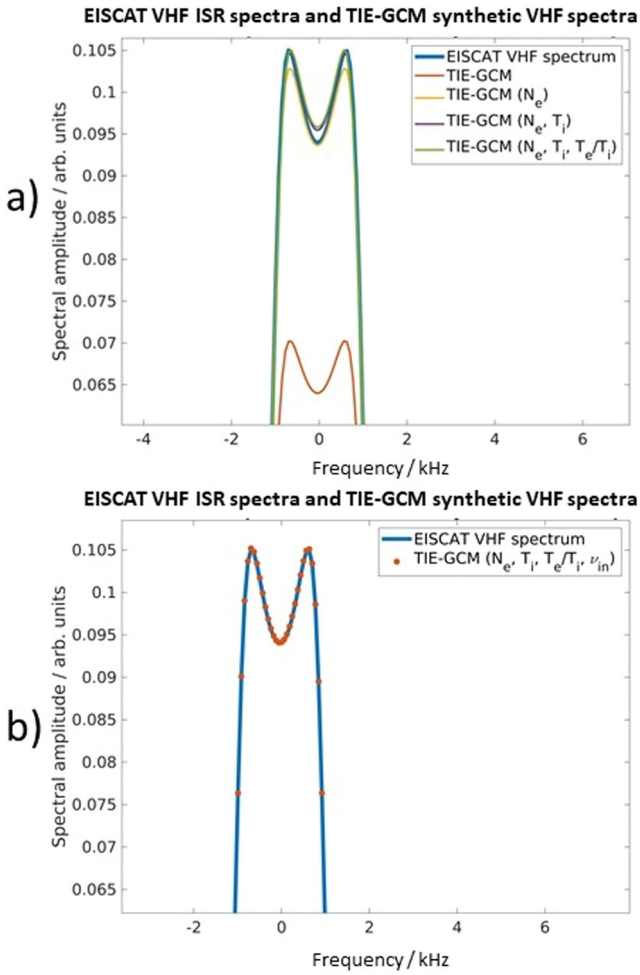

Figure 9. Same as Figure 8 but for VHF.

4.2. Assimilation of Measured Versus Fitted VHF Spectra

The investigations of the altitude-dependent impact of the actual fitted and a priori parameters in Section 3 have been conducted using the results of the GUISDAP incoherent scatter spectrum fit as the 'measured' spectrum. However, we have seen in Figure 2 that especially for EISCAT VHF ISR observations, the GUISDAP fitted spectra can deviate notably. This is most prevalent in the E region at 120 km, where the measured VHF spectrum does not show the classical double-peak shape of ISR spectra. However, the GUISDAP analysis forces the fitted spectrum into a double-peak shape. Such limitations of the GUISDAP analysis suggest that assimilation of actually measured spectra rather than fitted ones is beneficial, although more computationally expensive. However, the measurement noise and the ion-neutral collision frequency profile in the E region need to be considered carefully.

It has been shown in Section 3 that in the E region, the ion-neutral collision frequency ν_{in} is the a priori parameter that affects the incoherent scatter spectrum the most. Günzkofer et al. (2023) showed that the ν_{in} profile in the E region can deviate strongly from climatology profiles and also physics-based models do not cover the kilometer-scale variability with altitude. Hence, the evaluation of an assimilated incoherent scatter spectrum applying TIE-GCM collision frequencies might not be much more meaningful than applying an empirical a priori profile. Furthermore, the restriction in collision frequency to a priori values might be responsible for the forced double-peak shape observed in Figure 2. Figure 11 shows multiple measured, fitted, and synthetic EISCAT VHF spectra at 120 km altitude to illustrate the various problems that need to be solved and included to obtain a physical consistent forward model for data assimilation of the measured spectra. The measured spectra are evaluated with a simple non-linear least-square fit as in the previous section. Each synthetic spectrum is calculated assuming the collision frequency to be ν_{in}, $5 \cdot \nu_{in}$, $10 \cdot \nu_{in}$, and $20 \cdot \nu_{in}$ with ν_{in} being the collision frequency as given by the TIE-GCM.

Figure 11a shows the measured VHF spectrum at 09–10 UT, which is considerably more noisy than the integration window from 10 to 11 UT shown in Figure 2. This illustrates that when assimilating actually measured spectra, noise in the spectrum tail can have a major impact. Both the single-peak measured spectrum and the GUISDAP-fitted double-peak spectrum are shown. GUISDAP is a highly sophisticated incoherent scatter analysis software and can handle measurement noise very well. However, the noise strongly affects the simple non-linear least-square fit assuming $1 \cdot \nu_{in}$. Therefore we will apply a step function filter that sets the spectral amplitude to zero at $|f| \gtrsim 2$ kHz. Figure 11b shows the measured spectrum and the four synthetic spectra. It can be seen, that all four synthetic spectra show the one-peak shape when no restrictions are set to the main plasma parameters N_e, T_e, T_i, and T_e/T_i. The parameters associated with the synthetic spectra in Figure 11b are shown in Figures 12a–12d.

Our results indicate that though all synthetic spectra in Figure 11b fit the measured spectrum, the associated plasma parameters need to be evaluated carefully. For the $\nu'_{in} = 20 \cdot \nu_{in}$ case, Figures 12a–12d show that the plasma parameters strongly deviate from the default values and especially the high T_e/T_i ratio is most likely nonphysical in the E region. On the other hand, the $\nu'_{in} = \nu_{in}$ and $\nu'_{in} = 5 \cdot \nu_{in}$ cases show $T_e/T_I \ll 1$ which is also highly unusual and potentially nonphysical. However, a non-Maxwellian ion velocity distribution would affect the incoherent scatter spectrum similar to an increased T_i and could lead to observed $T_e/T_i < 1$ (Raman et al., 1981). For reference, we restrict $T_e/T_i \geq 1$ during the non-linear linear least square fit and obtain the spectra in Figure 11c and the parameters in Figures 12e–12h. It can be seen that only the $\nu'_{in} = 20 \cdot \nu_{in}$ and $\nu'_{in} = 10 \cdot \nu_{in}$ synthetic spectrum fit the measured spectrum in this case. The plasma parameters obtained for the $\nu'_{in} = 10 \cdot \nu_{in}$ case deviate significantly from the default values but are within a reasonable range.

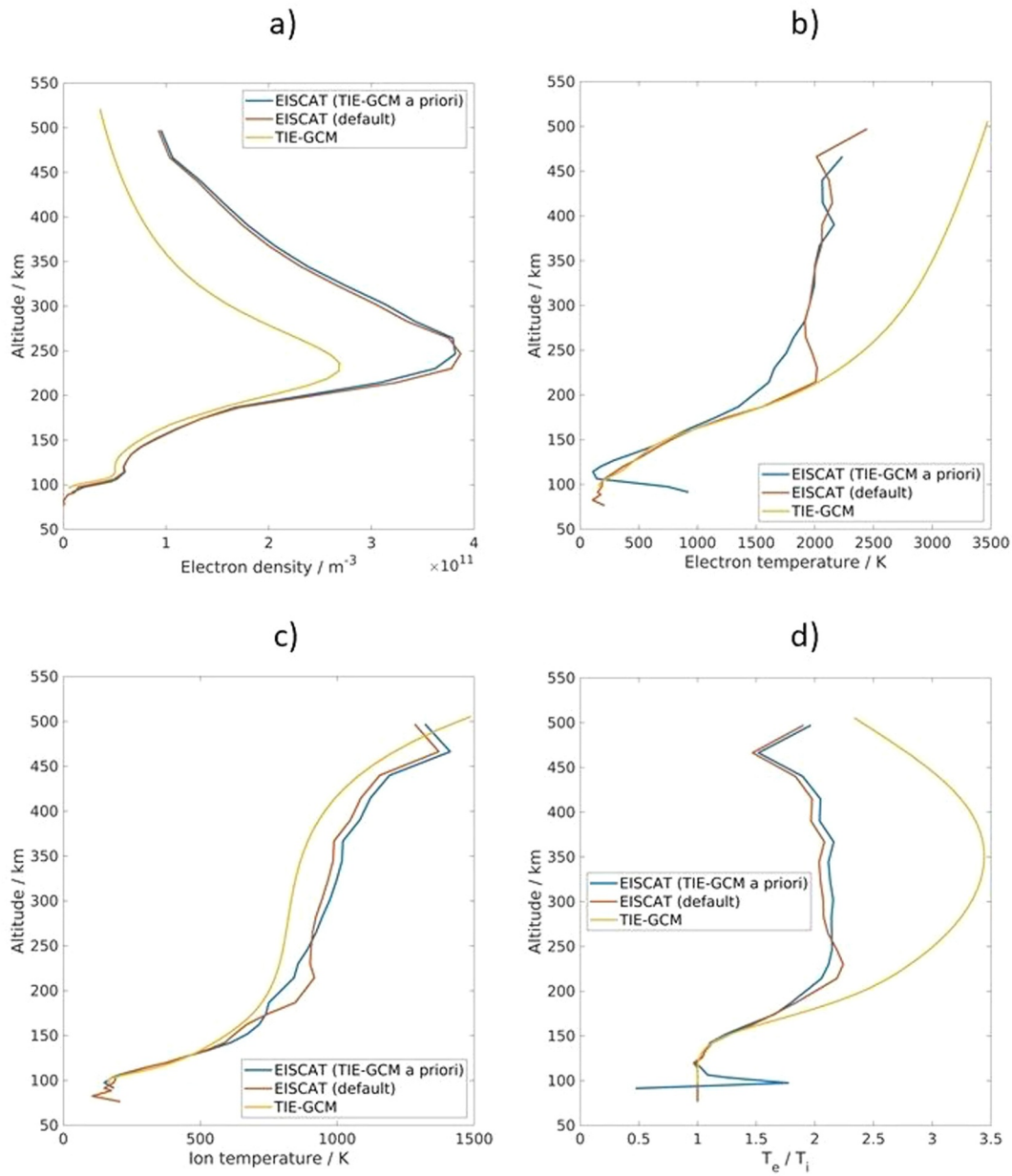

Figure 10. One-hour-mean profiles of the plasma parameters (a) electron density, (b) electron temperature, (c) ion temperature, and (d) ratio of electron-to-ion temperature from EISCAT UHF measurements and TIE-GCM. A second EISCAT UHF profile has been derived for each parameter by applying TIE-GCM profiles of the a priori parameters.

In summary, the default ion-neutral collision frequency values in combination with the common $T_e/T_i \geq 1$ assumption lead to strong differences between measured and fitted incoherent scatter spectrum. Hence, either the ion-neutral collision frequency is considerably larger than given by TIE-GCM or temperature ratios $T_e/T_i < 1$ occur due to non-Maxwellian ion velocity distributions. Following the results of Nygrén (1996) and Günzkofer et al. (2023), we suggest that a collision frequency in the range of $\nu'_{in} = 10 \cdot \nu_{in}$ is more likely, though this cannot be conclusively proven. A final answer to how to treat the assimilation of measured VHF incoherent scatter spectra is beyond the scope of the analysis presented in this paper. It can only be demonstrated that the E region physics needs to be better understood to limit the physical range of the spectrum interpretation.

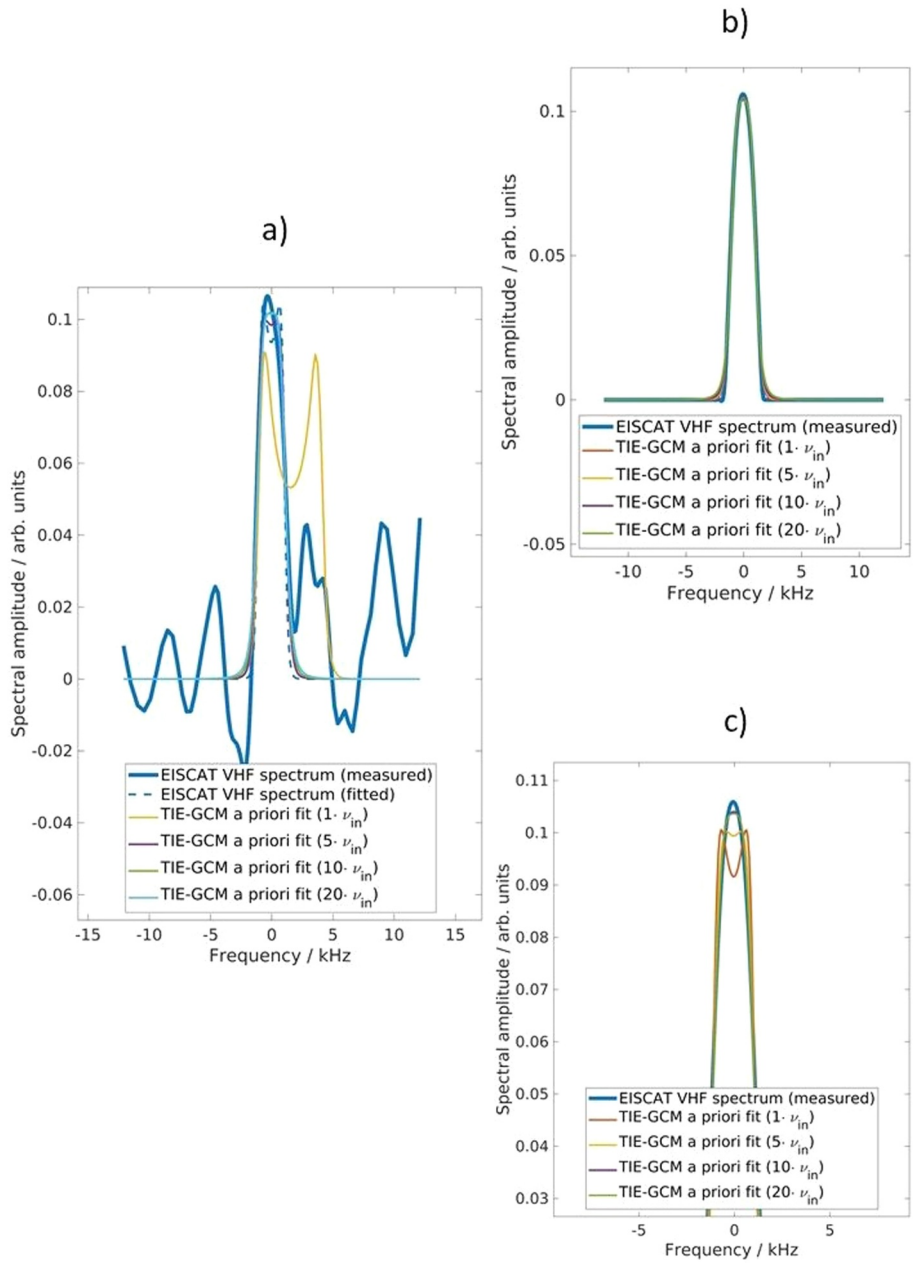

Figure 11. Measured, fitted, and synthetic VHF ISR spectra at 120 km altitude. (a) At 09–10 UT, it can be seen that strong noise at $|f| \gtrsim 2$ kHz in the ISR spectrum can impact the fitting quite significantly. This noise is removed by a step function filter. The filtered spectrum for 10–11 UT is fitted for different ion-neutral collision frequencies with (b) all parameters free and (c) $T_e/T_i \geq 1$ restricted.

5. Conclusions

In Section 1, three problems that arise with the assimilation of ISR-measured plasma parameters into ionosphere models have been identified. The solution to these problems would be to assimilate the incoherent scatter spectrum rather than single parameters inferred from it. Thereby, the parameter uncertainties arising due to the fitting process would not be assimilated into the model. Additionally, the a priori parameter (r_{O^+}, ν_{in}, and A) profiles could be treated consistently within the model after the assimilation process. The differences of the a priori parameter profiles between the model and the ISR analysis software would not affect the assimilation result. Lastly, multiple parameters could be assimilated via a mapping function to reduce calculation time.

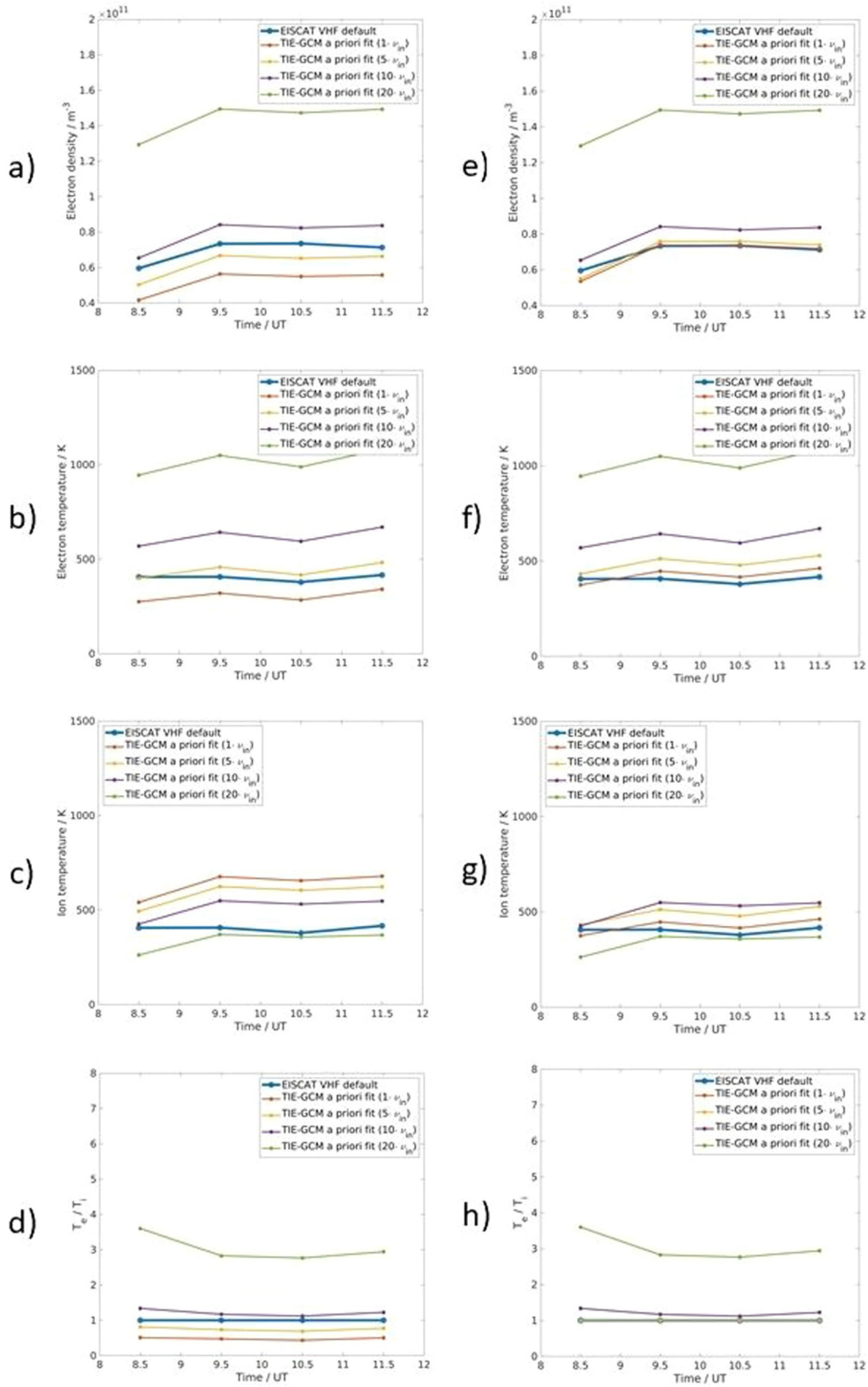

Figure 12. Plasma parameters at 120 km altitude obtained from the measured VHF ISR spectrum. (a)–(d) All parameters have been left free during the fitting (spectra shown in Figure 11b). (e)–(h) The restriction $T_e/T_i \geq 1$ is applied during the incoherent scatter fit (spectra shown in Figure 11c).

In this paper, we have investigated how synthetic incoherent scatter spectra calculated from TIE-GCM are affected by different parameters at various altitudes. For this purpose, we separated the parameters that generally affect the incoherent scatter spectrum in basic plasma parameters that are usually inferred from ISR measurements and a priori parameters that are taken from empirical models and act as a regularization constraint in the analysis. Concerning the three questions posed at the end of Section 3.1, we can give the following answers:

- The plasma temperatures have a visible impact on the incoherent scatter spectrum at all investigated altitude regions. However, we have seen that in the F2 region, where TIE-GCM gives a considerably larger T_e/T_i ratio than the EISCAT measurements, adapting T_e/T_i has a far larger impact on the synthetic spectra than adapting only the ion temperature. Whether this results in a potential problem for the assimilation of incoherent scatter spectra remains to be investigated.
- The impact of the a priori parameter profiles on the incoherent scatter spectrum is strongly different for the investigated altitude regions. We have shown that at the altitudes of the F2 region, the incoherent scatter spectrum is only affected by the standard plasma parameters N_e, T_e, and T_i and not by the profiles of the a priori parameters. At the altitudes of the F1 region, the ratio of atomic ions (mainly atomic oxygen) r_{O^+} strongly affects the incoherent scatter spectrum and we have seen that the EISCAT a priori and TIE-GCM profiles are very different. In the E region, the ion-neutral collision frequency ν_{in} was the a priori parameter with the highest impact on the incoherent scatter spectrum.
- In Figure 10, we have shown that the choice of a priori profile for r_{O^+} indeed affects the plasma parameters significantly. The strongest effect is found at about 200 km altitude, where the r_{O^+} profiles of the EISCAT a priori model and TIE-GCM deviate by a factor of about 40%. The maximum deviation of the electron temperature due to the reevaluation in Figure 10 is $\sim$300 K (or about 20%) which is nearly 40 times larger than the ΔT_e uncertainty given by the GUISDAP analysis.

We conclude that consistent handling of the different r_{O^+} profiles is only possible when assimilating the entire incoherent scatter spectrum. Assimilation of single parameters might be inaccurate causing model imbalances or physically inconsistent model states. Similar to r_{O^+} in the F1 region, varying ν_{in} profiles can only be treated consistently during assimilation when assimilating the entire incoherent scatter spectrum. Additionally, we investigated the sensitivity of the ISR plasma parameter fitting to varying collision frequencies, since previous studies indicated strong deviations of actual and modeled ν_{in} profiles. We found that due to the lower electron density and therefore lower signal-to-noise ratio (SNR) of ISR measurements in the E region, the impact of the collision frequency can be lower than the noise level. However, as consistency in ν_{in} is critical for assimilating incoherent spectra effectively, the in-model evaluation of the spectra needs to be able to handle low SNRs.

Though this paper aims to improve the assimilation of ISR measurements into physics-based atmosphere-ionosphere models, an actual assimilation is yet beyond its scope. This requires the development of 3DVAR or 4DVAR approaches for these type of models as it is done for middle atmosphere reanalysis or meteorological analysis (Eckermann et al., 2018; Gelaro et al., 2017; Kuhl et al., 2013). This paper presents a systematic identification of the possibilities and potential risks in changing ISR measurement assimilation from single parameters to entire incoherent scatter spectra. Hence, the next logical step will be testing the actual assimilation of incoherent scatter spectra. Assimilation of measurement data into the TIE-GCM has been performed with the *Data Assimilation Research Testbed (DART)* (Anderson et al., 2009; Elvidge & Angling, 2019). DART can also be applied in combination with other physics-based atmosphere-ionosphere models (Pedatella & Anderson, 2022). The general procedure would be to add a synthetic incoherent scatter spectrum as a variable to the model. This variable would then be assimilated with measured EISCAT spectra. As a first step, the assimilated incoherent scatter spectrum could then be evaluated in-model with a non-linear least-square fit to give the assimilated values for N_e, T_e, and T_i. Another conclusion that can be drawn from this paper is that EISCAT measurements such as the temperature profiles in Figure 3 need to be considered carefully. We cannot determine conclusively whether the r_{O^+} profile is correctly given by the EISCAT a priori model or the TIE-GCM (or likely neither). But assuming that the EISCAT a priori model is limited in accuracy, we have shown that the derived EISCAT ionospheric parameters can be significantly affected by the choice of a priori model.

Data Availability Statement

The GUISDAP software applied in this paper can be obtained from Häggström (2021). The data shown in this manuscript and the software required to reproduce the figures shown can be obtained from Günzkofer et al. (2024). All data and software are available under the Creative Commons Attribution 4.0 International license. In case of further questions about the data or the analysis software please contact the corresponding author.

Acknowledgments
EISCAT is an international association supported by research organizations in China (CRIRP), Finland (SA), Japan (NIPR and ISEE), Norway (NFR), Sweden (VR), and the United Kingdom (UKRI). The TIE-GCM and related Thermosphere-Ionosphere models have been developed by the "Atmosphere Ionosphere Magnetosphere" (AIM) Section of the High Altitude Observatory (HAO) at NCAR (see http://www.hao.ucar.edu/modeling/tgcm). The TIE-GCM data was generated on the computing servers of the DLR Institute for Solar-Terrestrial Physics in Neustrelitz. Gunter Stober is a member of the Oeschger Center for Climate Change Research (OCCR). The internal pre-review at DLR-SO by Helen Schneider is gratefully acknowledged. Open Access funding enabled and organized by Projekt DEAL.

References

Akbari, H., Bhatt, A., La Hoz, C., & Semeter, J. L. (2017). Incoherent scatter plasma lines: Observations and applications. *Space Science Reviews*, *212*(1–2), 249–294. https://doi.org/10.1007/s11214-017-0355-7

Anderson, J., Hoar, T., Raeder, K., Liu, H., Collins, N., Torn, R., & Avellano, A. (2009). The data assimilation research testbed: A community facility. *Bulletin of the American Meteorological Society*, *90*(9), 1283–1296. https://doi.org/10.1175/2009BAMS2618.1

Baumjohann, W., & Treumann, R. A. (1996). *Basic space plasma physics*. Imperial College Press. https://doi.org/10.1142/p015

Bilitza, D., Pezzopane, M., Truhlik, V., Altadill, D., Reinisch, B. W., & Pignalberi, A. (2022). The international reference ionosphere model: A review and description of an ionospheric benchmark. *Reviews of Geophysics*, *60*(4), e2022RG000792. https://doi.org/10.1029/2022RG000792

Chartier, A. T., Matsuo, T., Anderson, J. L., Collins, N., Hoar, T. J., Lu, G., et al. (2016). Ionospheric data assimilation and forecasting during storms. *Journal of Geophysical Research: Space Physics*, *121*(1), 764–778. https://doi.org/10.1002/2014JA020799

Eckermann, S. D., Ma, J., Hoppel, K. W., Kuhl, D. D., Allen, D. R., Doyle, J. A., et al. (2018). High-altitude (0–100 km) global atmospheric reanalysis system: Description and application to the 2014 austral winter of the deep propagating gravity wave experiment (deepwave). *Monthly Weather Review*, *146*(8), 2639–2666. https://doi.org/10.1175/MWR-D-17-0386.1

Elvidge, S., & Angling, M. J. (2019). Using the local ensemble Transform Kalman Filter for upper atmospheric modelling. *Journal of Space Weather and Space Climate*, *9*, A30. https://doi.org/10.1051/swsc/2019018

Folkestad, K., Hagfors, T., & Westerlund, S. (1983). EISCAT: An updated description of technical characteristics and operational capabilities. *Radio Science*, *18*(6), 867–879. https://doi.org/10.1029/RS018i006p00867

Gelaro, R., McCarty, W., Suárez, M. J., Todling, R., Molod, A., Takacs, L., et al. (2017). The modern-era retrospective analysis for research and applications, version 2 (MERRA-2). *Journal of Climate*, *30*(14), 5419–5454. https://doi.org/10.1175/JCLI-D-16-0758.1

Gjerloev, J. W. (2012). The SuperMAG data processing technique. *Journal of Geophysical Research*, *117*(A9), A09213. https://doi.org/10.1029/2012JA017683

Greenwald, R. A., Baker, K. B., Dudeney, J. R., Pinnock, M., Jones, T. B., Thomas, E. C., et al. (1995). Darn/Superdarn: A global view of the dynamics of high-lattitude convection. *Space Science Reviews*, *71*(1–4), 761–796. https://doi.org/10.1007/BF00751350

Günzkofer, F. (2024). *Impact of high-latitude atmosphere-ionosphere coupling on the space weather* PhD thesis. Ludwig-Maximilians-Universität München. https://doi.org/10.5282/edoc.33661

Günzkofer, F., Stober, G., Heymann, F., Tjulin, A., & Borries, C. (2024). Altitude-dependent plasma parameter variations of synthetic EISCAT UHF and VHF incoherent scatter spectra calculated from TIE-GCM results [Dataset and Software]. *Zenodo*. https://doi.org/10.5281/zenodo.13947114

Günzkofer, F., Stober, G., Pokhotelov, D., Miyoshi, Y., & Borries, C. (2023). Difference spectrum fitting of the ion-neutral collision frequency from dual-frequency EISCAT measurements. *Atmospheric Measurement Techniques*, *16*(23), 5897–5907. https://doi.org/10.5194/amt-16-5897-2023

Hagan, M. E., & Forbes, J. M. (2002). Migrating and nonmigrating diurnal tides in the middle and upper atmosphere excited by tropospheric latent heat release. *Journal of Geophysical Research*, *107*(D24), 4754. https://doi.org/10.1029/2001JD001236

Hagan, M. E., & Forbes, J. M. (2003). Migrating and nonmigrating semidiurnal tides in the upper atmosphere excited by tropospheric latent heat release. *Journal of Geophysical Research*, *108*(A2), 1062. https://doi.org/10.1029/2002JA009466

Häggström, I. (2016). *Gusidap 8.3*. EISCAT Scientific Assosciation. Retrieved from https://eiscat.se/wp-content/uploads/2016/08/GUISDAP.pdf

Häggström, I. (2021). Guisdap9. https://gitlab.com/eiscat/guisdap9.Gitlab

Heelis, R. A., Lowell, J. K., & Spiro, R. W. (1982). A model of the high-latitude ionospheric convection pattern. *Journal of Geophysical Research*, *87*(A8), 6339–6345. https://doi.org/10.1029/JA087iA08p06339

Hovland, A. Ø., Laundal, K. M., Reistad, J. P., Hatch, S. M., Walker, S. J., Madelaire, M., & Ohma, A. (2022). The Lompe code: A Python toolbox for ionospheric data analysis. *Frontiers in Astronomy and Space Sciences*, *9*, 412. https://doi.org/10.3389/fspas.2022.1025823

Hutchinson, I., & Freidberg, J. (2003). *Lecture notes in introduction to plasma physics I*. Plasma Science and Fusion Center, Massachusetts Insitute of Technology (MIT). Retrieved from https://ocw.mit.edu/courses/22-611j-introduction-to-plasma-physics-i-fall-2003/pages/lecture-notes/

Kuhl, D., Rosmond, T., Bishop, C., McLay, J., & Baker, N. (2013). Comparison of hybrid ensemble/4DVar and 4DVar within the NAVDAS-AR data assimilation framework. *Monthly Weather Review*, *141*(8), 2740–2758. https://doi.org/10.1175/MWR-D-12-00182.1

Laundal, K. M., Reistad, J. P., Hatch, S. M., Madelaire, M., Walker, S., Hovland, A. Ø., et al. (2022). Local mapping of polar ionospheric electrodynamics. *Journal of Geophysical Research: Space Physics*, *127*(5), e30356. https://doi.org/10.1029/2022JA030356

Lehtinen, M. S., & Huuskonen, A. (1996). General incoherent scatter analysis and GUISDAP. *Journal of Atmospheric and Terrestrial Physics*, *58*(1–4), 435–452. https://doi.org/10.1016/0021-9169(95)00047-X

Matsuo, T. (2020). Recent progress on inverse and data assimilation procedure for high-latitude ionospheric electrodynamics. In M. W. Dunlop & H. Lühr (Eds.), *Ionospheric multi-spacecraft analysis tools: Approaches for deriving ionospheric parameters* (Vol. 17, pp. 219–232). Springer Link. https://doi.org/10.1007/978-3-030-26732-2_10

Mehta, P. M., & Linares, R. (2018). A new transformative framework for data assimilation and calibration of physical ionosphere-thermosphere models. *Space Weather*, *16*(8), 1086–1100. https://doi.org/10.1029/2018SW001875

Navon, I. M. (2009). Data assimilation for numerical weather prediction: A review. In S. K. Park & L. Xu (Eds.), *Data assimilation for atmospheric, oceanic and hydrologic applications* (pp. 21–65). Springer Berlin Heidelberg. https://doi.org/10.1007/978-3-540-71056-1_2

Negale, M., Holmes, J., Parris, R., Ober, D., Dao, E., Kelly, R., et al. (2020). Using data assimilation to reconstruct high-latitude polar cap patches. *Radio Science*, *55*(6), e2019RS006937. https://doi.org/10.1029/2019RS006937

Nygrén, T. (1996). Studies of the E-region ion-neutral collision frequency using the EISCAT incoherent scatter radar. *Advances in Space Research*, *18*(3), 79–82. https://doi.org/10.1016/0273-1177(95)00843-4

Palmroth, M., Grandin, M., Sarris, T., Doornbos, E., Tourgaidis, S., Aikio, A., et al. (2021). Lower-thermosphere-ionosphere (LTI) quantities: Current status of measuring techniques and models. *Annales Geophysicae*, *39*(1), 189–237. https://doi.org/10.5194/angeo-39-189-2021

Pedatella, N. M., & Anderson, J. L. (2022). The impact of assimilating COSMIC-2 observations of electron density in WACCMX. *Journal of Geophysical Research: Space Physics*, *127*(1), e29906. https://doi.org/10.1029/2021JA029906

Picone, J. M., Hedin, A. E., Drob, D. P., & Aikin, A. C. (2002). NRLMSISE-00 empirical model of the atmosphere: Statistical comparisons and scientific issues. *Journal of Geophysical Research*, *107*(A12), 1468. https://doi.org/10.1029/2002JA009430

Rabier, F. (2005). Overview of global data assimilation developments in numerical weather-prediction centres. *Quarterly Journal of the Royal Meteorological Society*, *131*(613), 3215–3233. https://doi.org/10.1256/qj.05.129

Raman, R. S. V., St-Maurice, J. P., & Ong, R. S. B. (1981). Incoherent scattering of radar waves in the auroral ionosphere. *Journal of Geophysical Research*, *86*(A6), 4751–4762. https://doi.org/10.1029/JA086iA06p04751

Rawer, K., Bilitza, D., & Ramakrishnan, S. (1978). Goals and status of the international reference ionosphere. *Reviews of Geophysics and Space Physics*, *16*(2), 177–181. https://doi.org/10.1029/RG016i002p00177

Rees, D., & Fuller-Rowell, T. J. (1988). The CIRA theoretical thermosphere model. *Advances in Space Research*, *8*(5–6), 27–106. https://doi.org/10.1016/0273-1177(88)90039-7

Richmond, A. D., & Kamide, Y. (1988). Mapping electrodynamic features of the high-latitude ionosphere from localized observations: Technique. *Journal of Geophysical Research*, *93*(A6), 5741–5759. https://doi.org/10.1029/JA093iA06p05741

Richmond, A. D., Ridley, E. C., & Roble, R. G. (1992). A thermosphere/ionosphere general circulation model with coupled electrodynamics. *Geophysical Research Letters*, *19*(6), 601–604. https://doi.org/10.1029/92GL00401

Saponaro, J. A., & Copps, S. L. (1970). Operations and functions of the Apollo guidance computer during rendezvous. *IFAC Proceedings Volumes*, *3*(1), 116–135. https://doi.org/10.1016/S1474-6670(17)68772-X

Schunk, R. W., Scherliess, L., Eccles, V., Gardner, L. C., Sojka, J. J., Zhu, L., et al. (2016). Space weather forecasting with a multimodel ensemble prediction system (MEPS). *Radio Science*, *51*(7), 1157–1165. https://doi.org/10.1002/2015RS005888

Schunk, R. W., Scherliess, L., Eccles, V., Gardner, L. C., Sojka, J. J., Zhu, L., et al. (2014). Ensemble modeling with data assimilation models: A new strategy for space weather specifications, forecasts, and science. *Space Weather*, *12*(3), 123–126. https://doi.org/10.1002/2014SW001050

Suddath, J. H., Kidd, R. H., III, & Reinhold, A. G. (1967). *A linearized error analysis of onboard primary navigation systems for the Apollo lunar module* (Tech. Rep.). National Aeronautics and Space Administration. Retrieved from https://ntrs.nasa.gov/api/citations/19670025568/downloads/19670025568.pdf

Tjulin, A. (2022). *Eiscat experiments* (Tech. Rep.). EISCAT Scientific Association. Retrieved from https://eiscat.se/wp-content/uploads/2022/02/Experiments_v20220203.pdf

Yue, X., Wan, W., Liu, L., Zheng, F., Lei, J., Zhao, B., et al. (2007). Data assimilation of incoherent scatter radar observation into a one-dimensional midlatitude ionospheric model by applying ensemble Kalman filter. *Radio Science*, *42*(6), RS6006. https://doi.org/10.1029/2007RS003631